

Article

Self-Diffusion of Individual Adsorbed Water Molecules at Rutile (110) and Anatase (101) TiO₂ Interfaces from Molecular Dynamics

Stephanie J. Boyd ¹, Dáire O'Carroll ¹, Yogeshwaran Krishnan ², Run Long ³ and Niall J. English ^{1,*}

¹ School of Chemical and Bioprocess Engineering, University College Dublin, D04 V1W8 Dublin, Ireland; stephanie.deoliveirajardim@ucdconnect.ie (S.J.B.); daire.ocarroll@ucdconnect.ie (D.O.)

² Department of Energy Conversion and Storage Atomic Scale Materials Modelling, DTU Orbit, Technical University of Denmark, 2800 Kongens Lyngby, Denmark; yogkr@dtu.dk

³ Key Laboratory of Theoretical and Computational Photochemistry, Ministry of Education, College of Chemistry, Beijing Normal University, Beijing 100875, China; runlong@bnu.edu.cn

* Correspondence: niall.english@ucd.ie

Abstract: The distribution of individual water molecules' self-diffusivities in adsorbed layers at TiO₂ surfaces anatase (101) and rutile (110) have been determined at 300 K for inner and outer adsorbed layers, via classical molecular-dynamics methods. The layered-water structure has been identified and classified in layers making use of local order parameters, which proved to be an equally valid method of “self-ordering” molecules in layers. Significant distinctness was observed between anatase and rutile in disturbing these molecular distributions, more specifically in the adsorbed outer layer. Anatase (101) presented significantly higher values of self-diffusivity, presumably due to its “corrugated” structure that allows more hydrogen bonding interaction with adsorbed molecules beyond the first hydration layer. On the contrary, rutile (110) has adsorbed water molecules more securely “trapped” in the region between Ob atoms, resulting in less mobile adsorbed layers.

Keywords: molecular dynamics; self-diffusion; interfacial structures mobility; water molecules



Citation: Boyd, S.J.; O'Carroll, D.; Krishnan, Y.; Long, R.; English, N.J. Self-Diffusion of Individual Adsorbed Water Molecules at Rutile (110) and Anatase (101) TiO₂ Interfaces from Molecular Dynamics. *Crystals* **2022**, *12*, 398. <https://doi.org/10.3390/cryst12030398>

Academic Editor: Francesco Montalenti

Received: 19 January 2022

Accepted: 11 March 2022

Published: 15 March 2022

Publisher's Note: MDPI stays neutral with regard to jurisdictional claims in published maps and institutional affiliations.



Copyright: © 2022 by the authors. Licensee MDPI, Basel, Switzerland. This article is an open access article distributed under the terms and conditions of the Creative Commons Attribution (CC BY) license (<https://creativecommons.org/licenses/by/4.0/>).

1. Introduction

Since Fujishima and Honda stated the possibility of producing hydrogen and oxygen gas from water splitting when exposing titanium dioxide (TiO₂, known popularly as titania) to light irradiation [1], and, attributed to its non-toxicity and natural abundance, TiO₂ has been widely investigated for various promising renewable energy applications using photo-electrochemical dissociation [2–4]. Unfortunately, even after almost a half-century of studies in the area of photoelectrochemical (PEC) water splitting, the fundamental physics and chemistry behind it remains poorly understood [1], as well as the ideal and most efficient semiconductors not yet found.

From the naturally occurring TiO₂ polymorphs, the far more important facets are rutile (110) and anatase (101) [5,6]—where anatase demonstrates superior photocatalytic activity [7] and the (101) surface happens to be the predominant and that one with the lowest-energy surface of anatase TiO₂ [8], owing to its metastable nature, commonly seen in nanomaterials, whilst rutile presents greater thermodynamic stability phase in bulk [9,10]. Their properties and behavior are crucial to understanding TiO₂/water interfaces, the structure and “self-ordering” of water at various metal-oxide surfaces; specifically intrinsic surfaces and water molecules in the interfacial and confined region, as well fine-tuning catalytic applications [11].

Molecular dynamics, amongst various other approaches, is considered a valuable and effective tool to characterize the vibrational and dynamical behavior of water molecules on TiO₂ surfaces such rutile (110) and anatase (101) [12,13]. In particular, adsorption forms

of water on anatase (101) have been studied in much detail using ab initio MD (AIMD) to understand the librational motion of adsorbed water more thoroughly [13,14]. In recent years, as the system has been quickly developed, studies of modern models' potentials [15] and clustering of water layers [16,17] at TiO₂ interfaces using DFT-based ab initio molecular dynamics (AIMD) have been reported. Although in terms of analysing layered diffusion in small systems this can be significantly more challenging than MD, as it calculates layered water diffusion from the small system sizes available to AIMD. When we look at molecular absorption in MD, however, we see most published works, in fact, state that this absorption is more energetically favourable at both low and monolayer coverage, even though there is still a limited understanding of TiO₂/water interfaces overall.

There have been apparently more studies on rutile (110)–water interfaces regarding the confinement of water molecules and their mobility. Ion adsorption of rutile (110) was reported by Zhang et al. [18], whereas the electric double layer structure has recently been probed by Predota et al. [19]. Many other theoretical studies have been systematically investigated on this surface, such as the nature of layered water structure [20] ionic adsorptions [21] viscosity and self-diffusion of the water layers and dielectric properties of the interface. As one of the particular interest areas of study of the authors, diffusivity was reported to increase further away from the surface going toward bulk-like values [22] which is in accordance with the experimental measurements of Mamontov et al. [23,24].

In this study, we present results, obtained rigorously from equilibrium classical molecular dynamics simulations at 298 K of self-diffusivity of inner and outer layers of both anatase (101) and rutile (110). This is a directly observable property that provides a significant comparison between the dynamics of the semiconductor and its adsorbed layers, allowing the studies of interactions between them and providing interesting insights regarding mobility and water break-up events. Furthermore, we provide the distribution of self-diffusivities of individual water molecules in the inner and outer layers at TiO₂ surfaces to highlight the complex nature of distinct molecular behaviour from immobile adsorbed water molecules to more mobile and flimsy bounded water. A vital point for the analysis of structural and dynamical properties of interfacial water, such as self-diffusivity, is to assure simulation times will have a long and adequate length, as well as favorable statistics when utilizing well-tested empirical potentials [25]. This is, in fact, one of the main concerns of the authors here, as suitable simulation length will allow proper convergence for both surfaces and the achievement of meaningful insights with regard to layered water molecules diffusivity.

Here, we explore self-diffusion, which is a dynamical property of central importance for electrochemical applications in water/metal-oxide interfaces. In detail, we describe the probability distribution of self-diffusion of individual water molecules in adsorbed layers, as well as the distinct differences between anatase and rutile in disturbing and shifting these molecular distributions. The present statistical and individual-molecule analysis has been explored in previous work using MD simulations for the polarized and rigid water model TIP4P-2005 by some of the authors [26] and, it apparently continues to be a rather overlooked field of study in molecular fluids' transport properties. To the best of the authors' knowledge, individual self-diffusivities (from mean squared displacements) were previously investigated in the context of heterogeneous molecular behaviour regarding hydration layers around proteins [27], and in water adsorption at single-molecule to fully surface coverage [16,28], although no residence times of water molecules in different layers were analysed in detail. The present study elucidates water dynamics in a single-molecule point of view, and it gives a better understanding of the structural and dynamical properties changes of individual water molecules at interfaces rather important in solar-energy conversion applications applying a distinct layering ordering method based in a combined hydrogen-bonding analysis and local order parameters (LOPs).

2. Computational Details

We have carried out equilibrium classical molecular dynamics simulations on systems containing models of TiO₂ anatase (101) and rutile (110) surfaces based on the Leapfrog Verlet algorithm [29]. 2000 water molecules were accommodated in supercells containing 448 TiO₂ units of each model under orthogonal periodic boundary conditions. These cells were expanded in the z-direction perpendicular to the surface such that the bulk density was ~1 g/cm³. The particle-mesh Ewald (SPME) summation [30] was employed to evaluate long-range electrostatics, with a cutoff distance of 9 Å, as listed in [31]. All analyses were performed over 300 ps intervals of a 1 ns trajectory, considering the first 50 ps of each sub-interval for layers identification where a minimum length of MSD and statistical sampling level was defined in order to ensure formation of the Fickian regime in the region [32]. The single point charge, flexible water SPC/fw model [33] was chosen to represent water here due to its capability in reproducing liquid water structure appropriately, and, especially diffusivity, and dielectric properties in various temperature and density conditions [33]. The SPC/fw water model was also preferred because of its considerably superior estimation of self-diffusivities [34] and freezing point for water [35] facing the SPC model. All simulations were performed in the microcanonical NVE ensemble using the DL-POLY Classic software package [36] after thermal equilibration in the NVT ensemble for a period of 100 ps, using the Nosé-Hoover thermostat at initial conditions of 298 K. A time step of 0.25 fs was chosen to avoid thermal and pressure accumulation in NVE production simulations. The cell dimensions and other simulation parameters are described in Table 1, and snapshots of equilibrated interfacial structures are shown in Figure 1.

Table 1. Details of the systems used in this work.

| Surface | x, y, z (Å) | NTiO ₂ | NH ₂ O | T (K) |
|--------------------|------------------------|-------------------|-------------------|-------|
| Anatase (101) [31] | 26.495, 40.956, 69.873 | 448 | 2000 | 298 K |
| Rutile (110) [31] | 23.624, 45.381, 69.450 | 448 | 2000 | 298 K |
| Bulk water | 30.00, 30.00, 30.00 | 0 | 826 | 298 K |

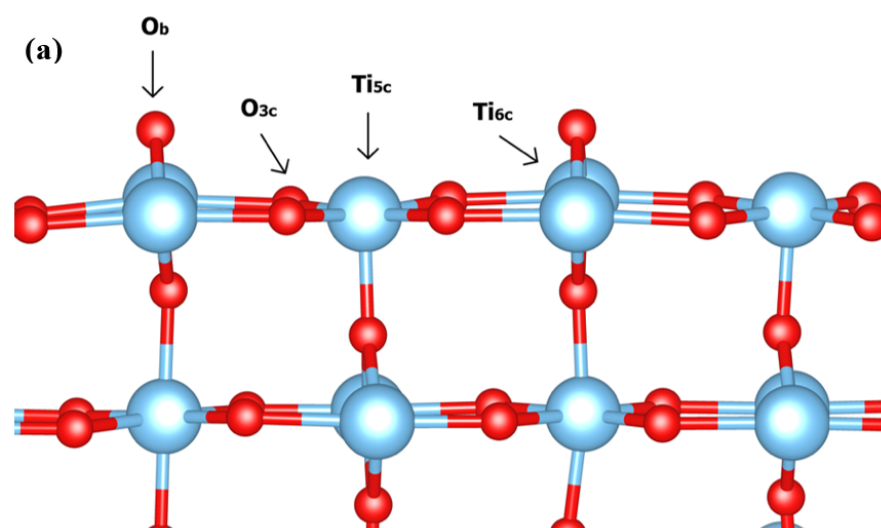


Figure 1. Cont.

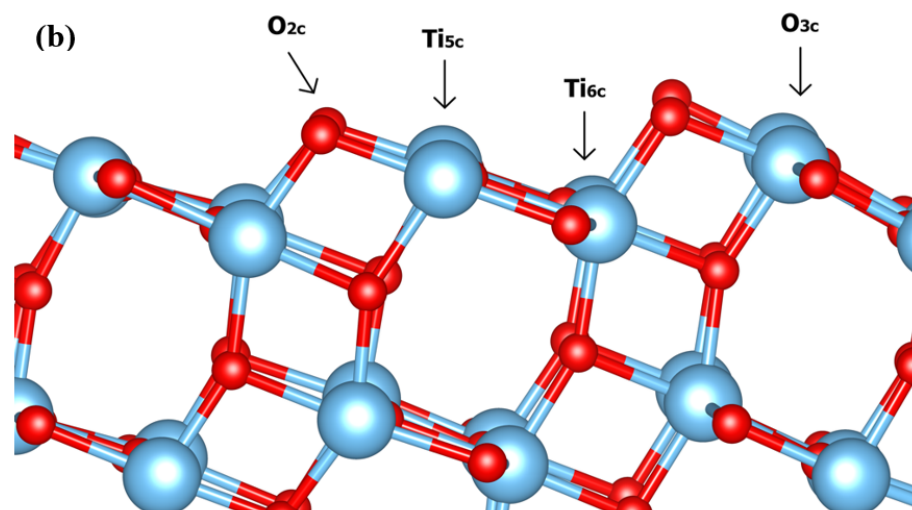


Figure 1. Structure of TiO_2 surfaces in the z -direction (a) rutile (110) and (b) anatase (101). Where O_b is a bridging oxygen, O_{3c} a three-coordinated surface oxygen, Ti_{5c} a penta-coordinated surface Ti atom, and Ti_{6c} a hexa-coordinated Ti atom.

Due to its suitable performance for titania [37–41], the systems were described by Matsui and Akaogi’s [42] empirical potential for TiO_2 which involves Buckingham-type interactions with parameters reported by Bandura et al. [43] and Predota et al. [20] Using these potentials has resulted in valuable insights regarding vibrational density of states, as well as hydrogen-bonding properties on TiO_2 –water interfaces [34]. Reactive force-fields were also considered as a valid and good option for this work and, were in fact, adopted before for water– TiO_2 interfaces analysis [44]. However, the authors are not focusing on water splitting or OH dissociation, but are rather interested in water mobility within adsorbed layers itself. The non-dissociative Matsui–Akaogi model proved to be a more appropriate choice as it allows both applicability and reliability to large-scale simulations [38,40], especially when associated with a flexible water model which it is expected to provide realistic description of water interactions with the surface.

In order to meaningfully define transient sub-phases such as layers in the simulation, we employed a method combining hydrogen-bonding analysis and local order parameters (LOPs) techniques commonly used in nucleation studies [45,46]. This method was first proposed in an earlier paper by some of the authors [47] as an efficient tool for interface analysis and is used effectively here to illustrate the difference in the chemical and physical properties of water molecules in various environments close to the interface and in the condensed bulk phase.

Hydrogen bond analysis was carried out using the method of Luzar and Chandler [48] which considers the geometric relationship between donor and acceptor atoms. For a donor molecule D-H and an acceptor atom A, the Luzar-Chandler conditions define a hydrogen bond as occurring when the following conditions are satisfied:

$$r_{D-A} \leq 3.5 \text{ \AA} \text{ and } D_{HA} \leq 30^\circ \quad (1)$$

Using these criteria, water molecules in the bulk phase have an average of 3.5 hydrogen bonds, whereas water molecules in interfacial layers have either 2 or 4 hydrogen bonds on average, depending on their proximity to the interface. Order parameters provide a means to quantify the “regularity” of a system for comparative purposes, e.g., to distinguish between different phases of a material [49]. LOPs represent the regularity of the environment around a particular molecule, taking into account the relative positions of first and second neighbors within a certain cut-off radius.

The LOPs are derived from Steinhardt classification parameters [46], which are defined below:

$$q_{lm}(i) = \frac{1}{N_{\text{neigh}}(i)} \sum_{j=1}^{N_{\text{neigh}}(i)} Y_{lm}(\theta_{ij}, \varphi_{ij}) \quad (2)$$

Here, i is a particle (i.e., water molecule) in the system, j are the neighbors of i (please note that in this study, neighbors are those within the 3.5 Å cut-off radius of the centre of mass of particle i), and $Y_{lm}(\theta_{ij}, \varphi_{ij})$ are spherical harmonics of order l and degree m , with θ_{ij} and φ_{ij} representing the azimuthal and altitudinal angle between particle i and j , respectively [47]. From this definition, the LOP terms are defined as:

$$\langle q_{lm}(i) \rangle = \frac{1}{N_{\text{neigh}}(i) + 1} \sum_{j=0}^{N_{\text{neigh}}(i)} q_{lm}(j) \quad (3)$$

where the $j = 0$ term in the sum represents the Steinhardt classification parameter of particle i itself. These $\langle q_{lm} \rangle$ terms are then summed over degrees m and normalized to yield the l th order local order parameter:

$$\langle q_l(i) \rangle = \left[\frac{4\pi}{2l+1} \sum_{m=-l}^l |\langle q_{lm}(i) \rangle|^2 \right]^{1/2} \quad (4)$$

The self-diffusion constant of water along xy plane (parallel to the surfaces) and z -direction (perpendicular thereto) at either surface was obtained from the Einstein relationship as the limiting slope from the mean-square displacement (MSD) [29,32]:

$$D_i = \frac{1}{2} \lim_{t \rightarrow \infty} \frac{\langle |r_i(t) - r(0)|^2 \rangle}{t} \quad (5)$$

where $r_i(t)$ represents the position of particle, i at time t . Following the technique used in an earlier paper by some of the authors [26], the MSD for *each individual molecule* contained in the first hydration layers of both anatase (101) and rutile (110) was determined—so as to study shifts in the probability distributions of the molecular self-diffusivities and mobility in the fully hydrated surface that is crucial for the photoinduced transfer at the water-TiO₂ interface [50] and further away the surface.

The MSDs and diffusivity of adsorbed layers were computed throughout independent subsections of the trajectory (1 ns) following a strict filtration process. Analysis was carried out over 300 ps sub-intervals of an overall 1 ns trajectory. Layered molecules were identified by computing the average fourth-order LOP ($\langle q_4 \rangle$) and number of hydrogen bonds (nH) for each water molecule in the system over the first 50 ps of the 300 ps sub-interval. These values were then used to construct a sample set of $\langle q_4 \rangle$ values, which we readily verified followed a two-tailed normal distribution, and from which the mean (μ) and standard deviation (σ) were calculated. Z-testing was used to identify molecules belonging to layers with 95% confidence, corresponding to $|\langle q_4(i) \rangle - \mu| \geq 1.96\sigma$. Molecules identified in this way were assigned to the inner layer if they had $nH \leq 2.5$ on average over the first 50 ps of the 300 ps analysis interval, and the outer layer otherwise. The MSDs of these sets of molecules were then calculated over various 300 ps sub-intervals to obtain reliable data for the calculation of self-diffusivity.

3. Results and Discussions

3.1. Dynamic Interfacial Structure and Layers Identification

To better comprehend the underlying adsorption on the surfaces, it is de rigueur to examine the density profiles along the surface. As reported in previous work of the authors O'Carroll and English [47], and also shown in Figure 2, the water density profile in the direction perpendicular to the surface plane (z) of the interfaces of both anatase (101) and

rutile (110) exhibit the surface adsorption occurring in layers at given distances from the surface (Δz). In any event, the layer itself can be identified by each space between two minima. Initially, it is possible to see an ordering effect where random water molecules are subjected to a layering transformation upon contact with the interface. These results agree well with literature, where the water close to the surface has a considerably ordered structure [28,31,47,51] and also explains why considerable high density is seen at the surface where water molecules seem to be packed in a differ manner than in bulk water [52]. In the interface region, rutile (110) shows two to three distinct-shaped peaks, whereas anatase (101) shows only two. This can be explained by the fact that in the anatase (101) surface water molecules remain in-between the O_{2c} atoms, strongly hydrogen-bonded to them, whilst weakly bonded to the Ti_{5c} surface atoms. On the other hand, the same does not occur for rutile, as water molecules occupy the spaces in between the Ti_{5c} , owing to markedly restricted ridges and insufficient inter-ridge volume for the adsorption to take place [37].

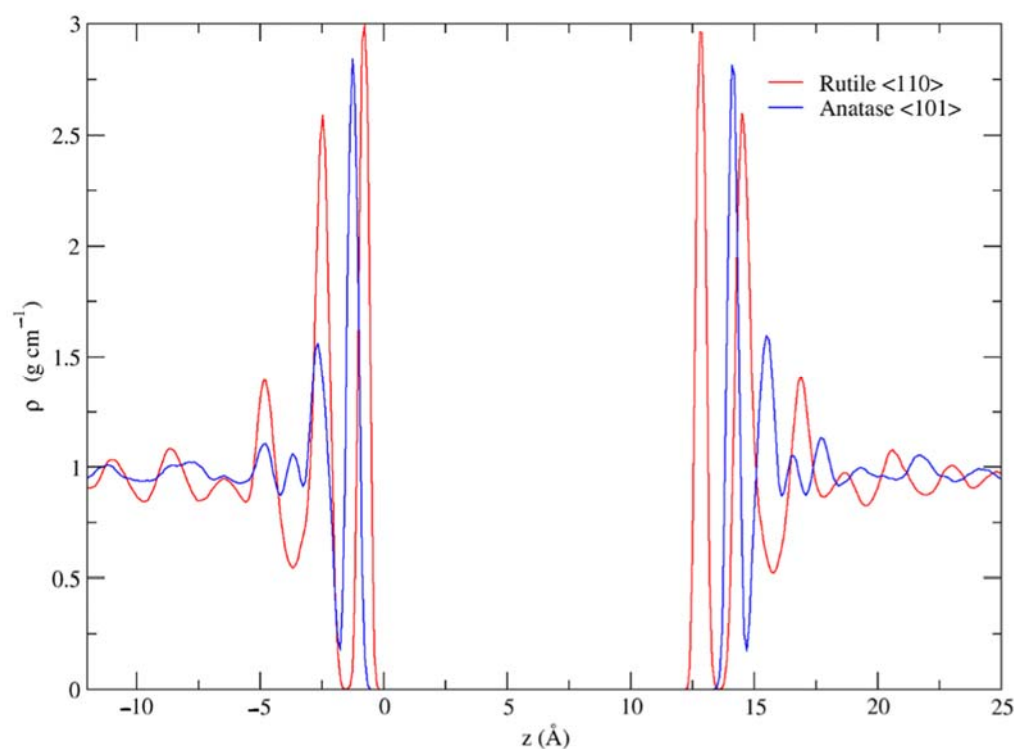


Figure 2. Density profile of adsorbed water molecules (g cm^{-3}) at TiO_2 surfaces along the z -direction.

It is important to note that the first distinct water molecule layer disseminating from the surface and limited by the second minima ($\Delta z = \sim 1.2 \text{ \AA}$ for anatase (101)) is, in fact, the “boundary” between the adsorbed monolayer and further layers from the surface—often referred as ‘ML’ or ‘1L’), followed by a second layer ‘2L’ ($\sim 2.4 < \Delta z < \sim 3.9 \text{ \AA}$) not connecting directly with the surface. After this distance, it is possible to see the density layers becoming less clear, showing a third less-distinct layer ‘3L’ ($\sim 3.9 < \Delta z < \sim 5.2 \text{ \AA}$); occurring then a transition to the bulk density just above 10 \AA . The authors even consider the idea of an electrostatic force in the vicinity of the surface being responsible for the formation of layers simply by the proximity to the surface, as reported by O’Carroll et al. [31]. In any event, this confirms that water close to the surface presents greater density and a highly ordered structure reaching out to about 10 \AA and then going towards a random orientation where the properties are closer to those of liquid bulk water, as reported in [51,52].

In this study, we will focus on water mobility arrangements between layers in the region ($0 < \Delta z < \sim 3.9 \text{ \AA}$) which we will call: inner Helmholtz layer IHL and outer Helmholtz layer OHL. In practice, the IHL would still be the edge between the adsorbed monolayer (1L) physically having slightly less than 2.0 hydrogen bonds on average at either surface.

The OHL and subsequent layers that are not in any direct contact with the surface; however, they present the average hydrogen bond numbers for the bulk region, as showed in Figure S1 in the supporting material.

3.2. Diffusivity and Mobility of Adsorbed Water Layers

In order to quantify the dynamics of water molecules and estimate the diffusive properties of water at the water-TiO₂ interface, we calculated the water self-diffusion coefficient (D) from the center-of-mass mean squared displacements [32] over a 1 ns trajectory by means of the Einstein relationship for both anatase (101) and rutile (110) first and second adsorbed layer, as well as the bulk region. In Table 2, it is possible to see the self-diffusivities of the defined density layers IHL and OHL in the xy plane (parallel to the surfaces) and z -direction (perpendicular thereto) at either surface for longer 300 ps intervals. The self-diffusivity of bulk water was also calculated for reference, and it was found to be $\sim 2.26 \times 10^{-9} \text{ m}^2 \text{ s}^{-1}$, whereas the experimental bulk-water value is reported to be $2.3 \times 10^{-9} \text{ m}^2 \text{ s}^{-1}$ in the literature [53].

Table 2. Self-diffusivities [$\times 10^{-9} \text{ m}^2 \text{ s}^{-1}$] (x, y, z) in adsorbed layer (IHL) and second layer (OHL) from each surface. The total self-diffusivity is given by the sum of the different laboratory directions.

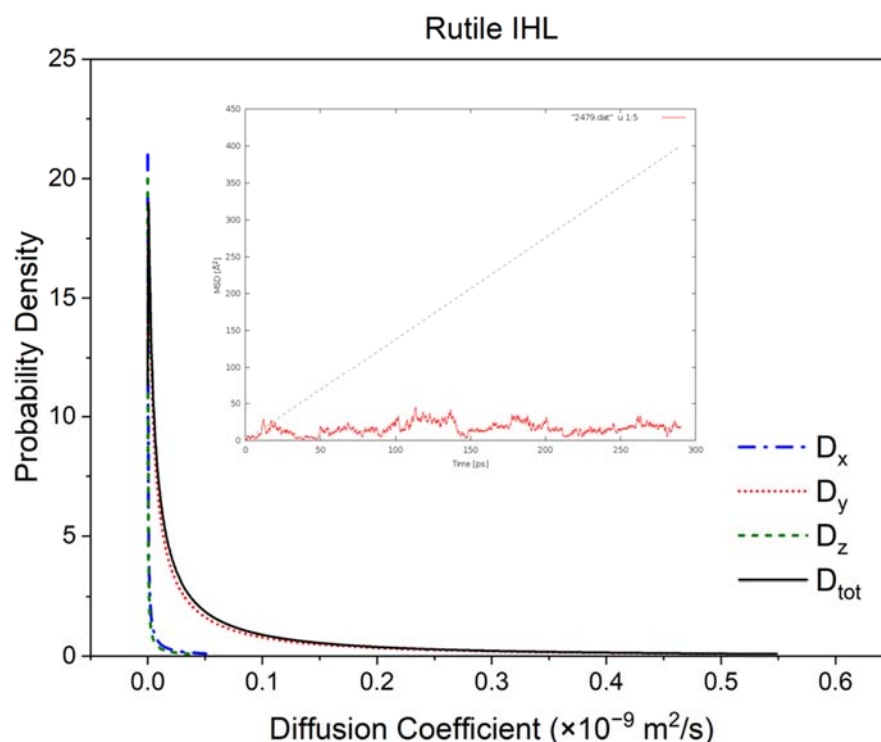
| Surface | IHL | OHL |
|---------------|---------------------|---------------------|
| Rutile (110) | 0.025, 0.027, 0.020 | 0.512, 0.545, 0.327 |
| Anatase (101) | 0.514, 0.522, 0.322 | 0.731, 0.720, 0.541 |

It was observed that the diffusion constants of the interfacial water differ from the bulk region by one order of magnitude, showing markedly lower values. Similar behaviour can be seen in Table S1 for self-diffusivities of anatase (101) in shorter 50 ps sub-intervals. This is an expected behavior since the first adsorbed layer is characterized by a certain confinement due to the interaction with the TiO₂ surface, in which case is bonded to surface oxygen O_{2c}/O_b atoms via coordination to unsaturated surface Ti_{4c}/Ti_{5c} atoms and H_w [54,55]. (cf. Figure 1) The comparison of normalized probability distributions for molecular self-diffusivities in the IHL and OHL for both anatase (101) and rutile (110) for the first 50 ps of the 300 ps sub-intervals are shown in Figure S2 (cf. Supplementary information), where some difference in the widths and the positions of the maxima is evident. The plots in Figure S2 are normalized such that the area under the curve represents the total number of water molecules present in the adsorbed layers. At first glance, we can see the high ordering effect in the IHL of both anatase (101) and rutile (110) considering the markedly inferior diffusivity values, whereas in the OHL water molecules are definitely less ordered, allowing a greater mobility. It is valid to say then the water molecules show inhomogeneous diffusive properties within distinct adsorbed layers: firmly adsorbed and sluggish in the IHL—especially in the rutile (110) surface, relatively mobile in OHL, and most mobile in the bulk region, which agrees well with experimental and theoretical results [51,56].

The OHL self-diffusion for both anatase (101) and rutile (110) leads to broader distributions, which reflects the tendency of diffusivity going towards bulk-values with increasing distance from the surface reported by Predotal et al. [22] Furthermore, when comparing the OHL of each surface, it is seen that rutile (110) shows considerably higher diffusivities values than anatase (101), which are reasonably close to the bulk region (cf. Table S2 in Supplementary Information). However, when we examine the residence time of rutile (110) IHL—specifically those molecules near Ti_{5c}—we see considerably small x, y, z components of the MSDs. The authors believe the great values of diffusivity in rutile (110) could be due incomplete binding or motion that was later negated due to the short 50 ps intervals; since the rutile (110) structure would suggest a rather opposite tendency regard OHL and, also considering its surface plane formed by Ti_{5c} rather than the bridging oxygen atoms O_b [37]. The mean square displacement of both surfaces for shorter 50 ps intervals illustrating these findings can be seen in Figure S3 in the supporting material.

As expected, anatase (101) IHL presents wider distribution than rutile (110) IHL, due to anatase-(101)'s triple-peaked and accessible structure that facilitates the formation of water hydrogen bonded in and beyond the adsorbed layer. Naturally, this greater level of mobility, or self-diffusion, in the adsorbed layer of anatase-(101), would result in increased photoactivity and water splitting rates, which it is the case for anatase-(101) [7] if compared with rutile (110). Surprisingly, it was not possible to identify molecules for diffusivity in the IHL of rutile (110) for all each first 50 ps of the sub-intervals. As rutile (110) molecules would just hop in and out very quickly it would be extremely difficult to ID them as their velocity autocorrelation goes to 0 nearly straight away, as illustrated in Figure S4 (cf. supporting material). This would suggest that the length of intervals might have been unfortunately not long enough to provide reliable results for self-diffusion of rutile (110). However, the probability distributions of rutile (110) showed that for all sub-intervals studied in this work, the water molecules in contact with the surface are relatively sluggish in the IHL (cf. Figure 3a and Figure S5 in the supporting material).

In attempt to correctly analyse self-diffusion in long enough sub-intervals and, considering all efforts to maintain the 90%-or-better occupancy filter used in this study, 300 ps sub-intervals of both anatase (101) and rutile (110) were carefully chosen to continue the analysis. Looking at long 300 ps MSD sub-intervals now, we see that rutile (110) leads to the narrowest distributions, which also shifts to lower values of the diffusion coefficient (cf. Figure 3). The findings can be tentatively explained by structural studies of anisotropic water orientations as the presence of bridging oxygen 'route' in rutile (110) impede diffusion motion of this layer along the surface. This, however, is not the case for anatase (101) surface (cf. Figure 4), where more similarity to bulk-like liquid conditions can be observed (cf. Figure 5) and were previously reported in the literature [39].



(a)

Figure 3. Cont.

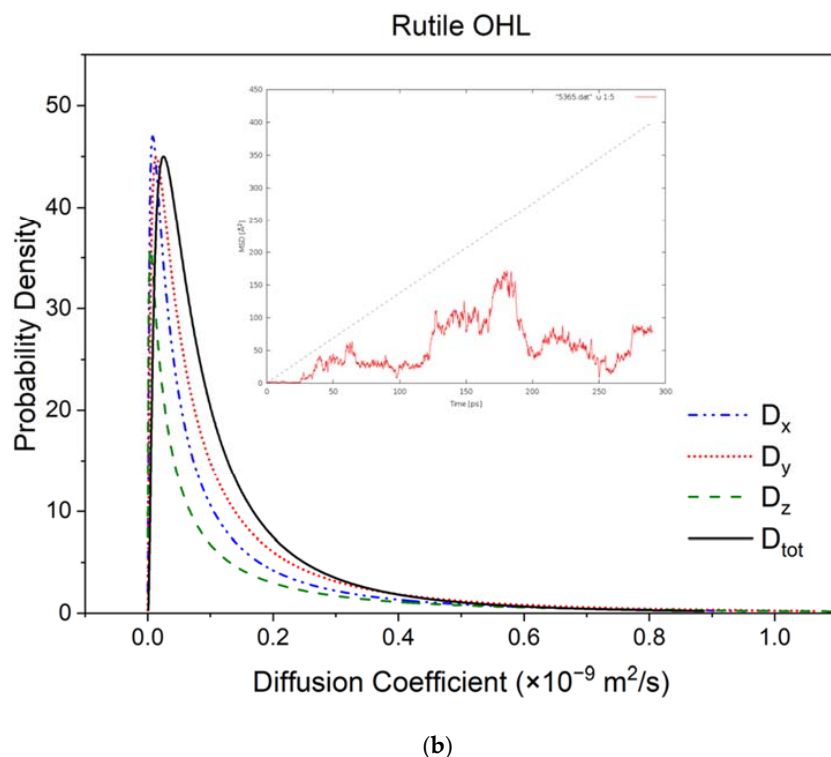


Figure 3. Probability distribution of self-diffusion coefficients of each individual water molecule averaged over 300 ps sub-intervals for rutile (110) (a) IHL (b) OHL. Diffusivities of the x , y , z directions are shown in blue, red and green dashed lines, respectively. The total diffusivity of individual molecules is represented by the solid black line. Note that these molecules are distinct from the average with 95% confidence. The MSD plotted in the graph refers to one individual water molecule present in both IHL and OHL, respectively. The self-diffusivity experimental value for bulk-water ($2.3 \times 10^{-9} \text{ m}^2 \text{ s}^{-1}$) is represented by the grey dotted line.

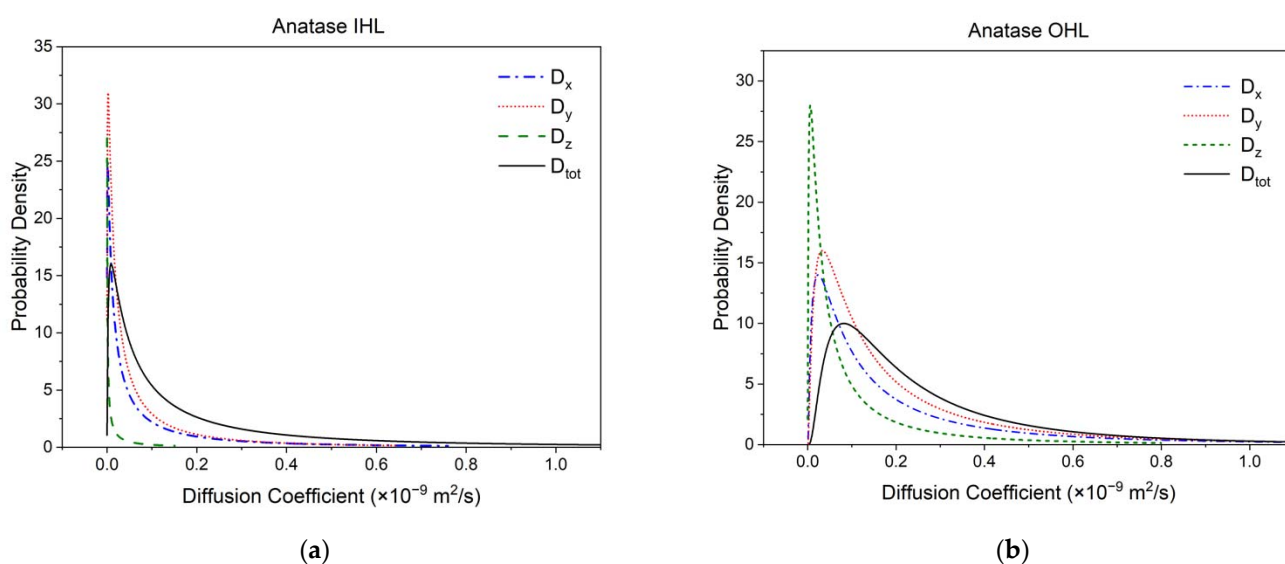


Figure 4. Probability distribution of self-diffusion coefficients of each individual water molecule averaged over a 300 ps sub-interval for anatase (101) (a) IHL (b) OHL. Note that these molecules are distinct from the average with 95% confidence. Diffusivities of the x , y , z directions are shown in blue, red and green dashed lines, respectively. The total diffusivity of individual molecules is represented by the solid black line.

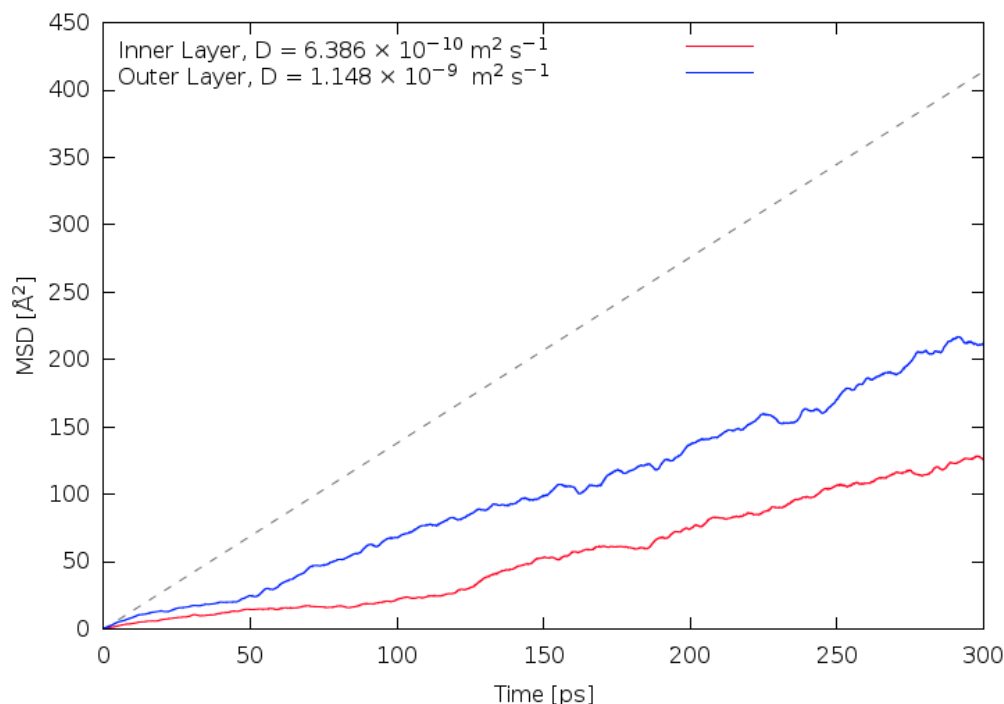


Figure 5. Mean square displacement (MSD) of water molecules in different layers at the water-TiO₂ anatase (110) interface for 300 ps sub-intervals. The self-diffusivity experimental value of $2.3 \times 10^{-9} \text{ m}^2 \text{ s}^{-1}$ for bulk-water—represented by the grey dotted line—is shown as reference.

It is once more seen that both OHL of anatase (101) and rutile (110) present relatively higher diffusivity than IHL in direct contact with the surface of TiO₂. The IHL of rutile (110) shows the sharpest distribution at $\sim 0.015 \times 10^{-9} \text{ m}^2 \text{ s}^{-1}$. As the distributions start broadening for both anatase (101) and rutile (110) OHL, it is possible to see the diffusivity rising and reaching values similar to those found in the bulk region due to the distance from the surfaces, as reported in the previous analysis of the first 50 ps of each sub-interval, also suggesting a smaller ordering effect in this case. These results likewise agree well with previous MD simulations for water in contact with rutile (110) carried out by Predota et al., and multi-layer water absorption studies by Mamontov et al. [23] describing the self-diffusivity of water increasing further away from the surface.

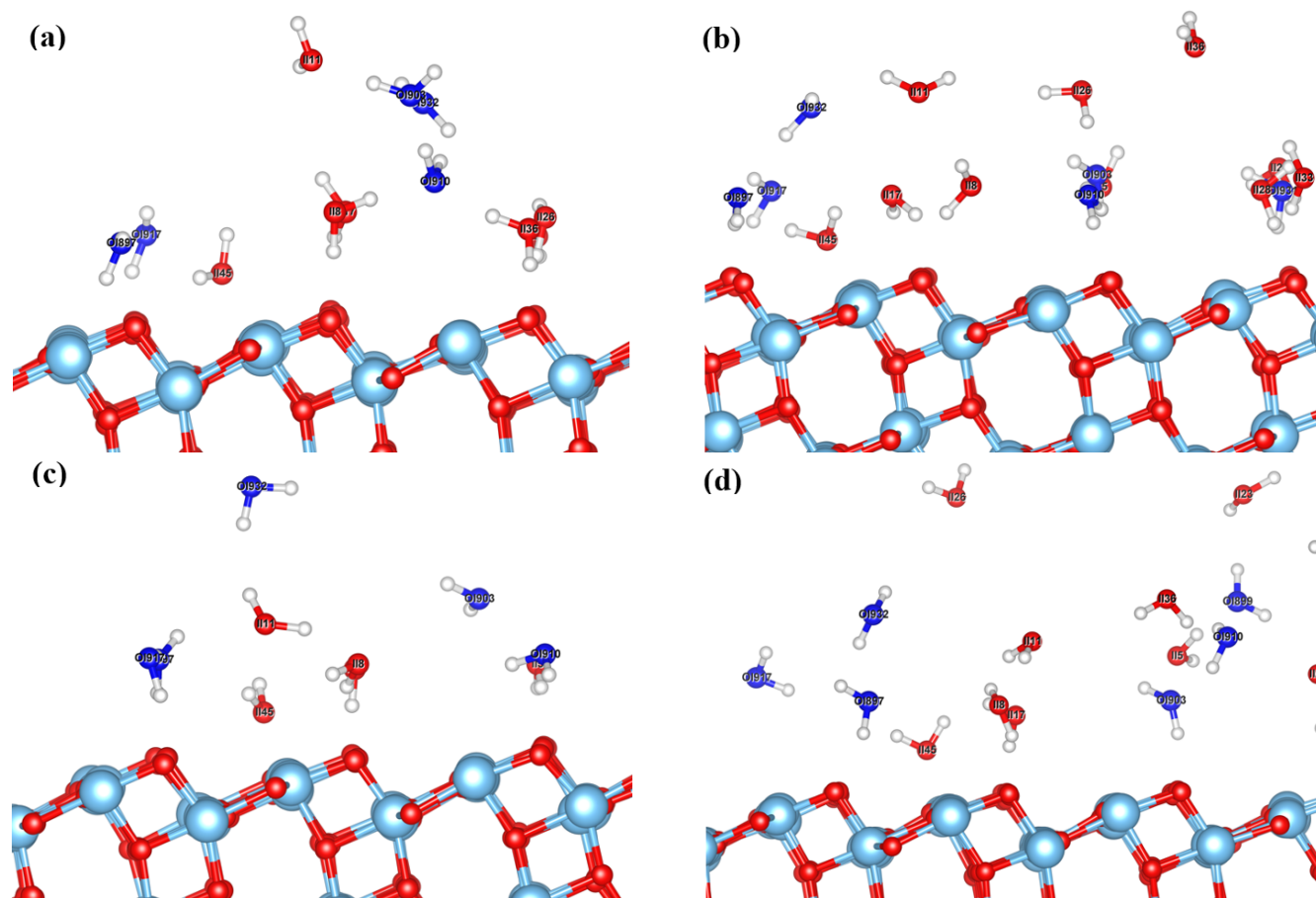
Looking closely at rutile (110) OHL (cf. Figure 3b), we see that the longer interval of 300 ps allowed better convergence as the self-diffusion now seems to be considerably smaller than the previous diffusivity presented for the first 50 ps of each 300 ps sub-interval. The wide self-diffusivity probability distribution of OHL showed in Figure S2 (cf. Supplementary information) shifted to a considerably narrower distribution as can be seen in Figure 3b, coming from values $\sim 0.98 \times 10^{-9} \text{ m}^2 \text{ s}^{-1}$ to $\sim 0.12 \times 10^{-9} \text{ m}^2 \text{ s}^{-1}$. If we then compare the OHL from rutile (110) and anatase (101) shown in Figures 3b and 4b, respectively, it is possible to see that rutile (110) now presents a markedly narrower probability distribution than anatase (101).

Similarly, rutile (110) surface IHL shows significantly low self-diffusion values, probably due to its atomistic construction (cf. Figure 1b) as adsorbed molecules are held very tightly and organized in the region close to surface atoms, against the more disarranged anatase (101) (cf. Figure 1a), as previously reported by English [41]. This, of course, makes rutile (110) less accessible to water molecules, allowing less hydrogen-bonding interactions between constrained water molecules and water molecules beyond the IHL. It is interesting to see in a similar manner individual water molecules diffusivity following the same tendency of averaged adsorbed water molecules reported in the literature [39]. This, nevertheless, can be related to hydrogen bonding patterns found in these distinct TiO₂ surfaces. Anatase (101) was reported to have 2.0 hydrogen bonds formed with water

molecules beyond the adsorbed layer, whereas rutile (101) presented roughly one per adsorbed water molecule—that means half of anatase (101) hydrogen bonds. This discrepancy stems from the less accessible architecture of the rutile (110) surface, resulting in lower diffusivity values due to the presence of bridging oxygen ridges along the surface, also observed in [39].

Another fundamental difference between IHL and further layers is basically $2.0 nH$, considering this layer's proximity to the TiO_2 surface, whereas OHL presents nH greater than the bulk. The hydrogen bonds for the studied surfaces here seem to agree well with experiments showing that bulk water has around 3.5 hydrogen bonds at 300 K [57]. (See Figure S2 in the Supplementary Information.)

We also suggest that the diffusivity values in the IHL show rather anisotropic characteristics as a result of the preferential motion along the ridges in the structure [41] (cf. Figures 1 and 6), which can somehow be confirmed by the similarity of self-diffusion values between both IHL of the surfaces for longer MSD sub-intervals presented in this study. Looking at anatase (101) IHL specifically, it is seen that diffusivity in the direction perpendicular to the rows of O_b is about 2 times higher than in the direction parallel to them, and 1 time higher than diffusivity away from the surface (cf. Table 2). This suggests a strong preference for the water molecules to move over or between the closely packed rows of O_b in anatase (101) rather than along them, contrary to intuition. However, for rutile (110) IHL, and considering particularly small diffusivity here, molecules would tend to be more mobile along the channel of Ti_{5c} (cf. Figure 3). It is worth noting that these values reflect the diffusivities of individual adsorbed water molecules identified in the IHL and OHL following an occupancy filter of 95% confidence.



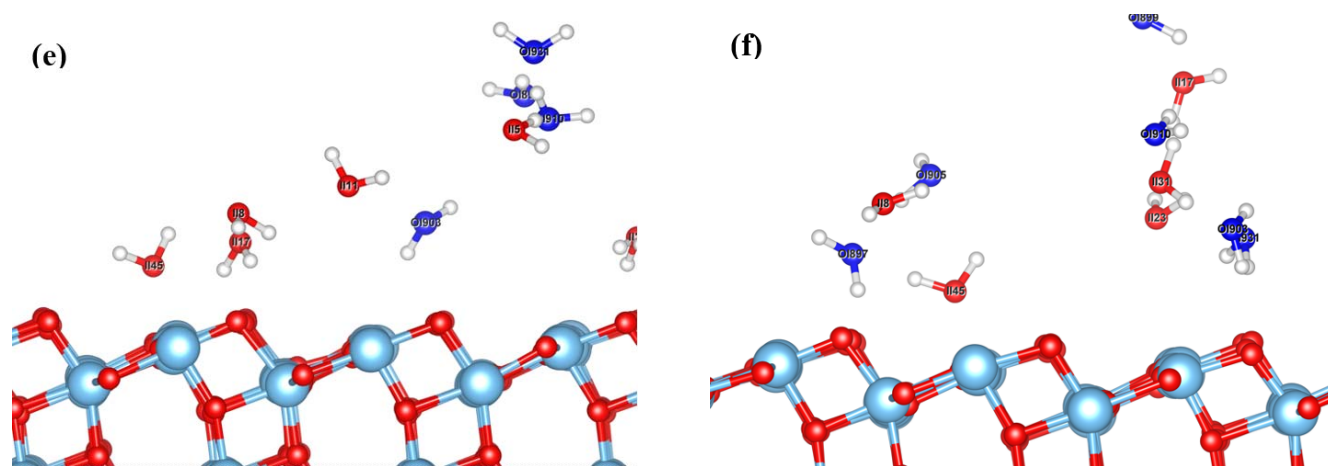


Figure 6. Snapshots of TiO_2 /water interfacial structures of anatase (101) at (a) 0, (b) 50, (c) 100, (d) 150, (e) 200 and (f) 300 ps, respectively. Titanium atoms are shown in light blue, TiO_2 oxygen atoms in red, water hydrogen in white, and water oxygen in red for IHL, and dark blue for OHL.

In Figure 6, it is possible to see snapshots of anatase (101) interface that shows this preferential motion of individual molecules not only the IHL, but also in the OHL. This anisotropic preference is also reflected in the coherency spectrum between the vibrational density of states of the IHL and Ob atoms at the rutile (110) [31]. To make an important clarification, the average LOP and number of hydrogen bonds over the chosen sub-interval is considered when determining whether a molecule is in the IHL or OHL; thus, molecules may migrate during the overall analysis period. In any event, we see that the diffusivities values increase as the distance from the surfaces also increases, likely to reach bulk-like values however (cf. Figure S5 in Supplementary Information), which proves that the layers identification method used in this study is successful and it can be potentially used for different types of analysis. Similar results were reported in previous molecular dynamics simulations for water in contact with rutile (110) and anatase (101) carried out by English [41] describing the self-diffusivity of water increasing further away from the surface. In contrast to the much less mobile and confined first IHL water molecules at rutile (110), the results agree well with the preliminary conclusion that accessible surface structure of anatase (101) in conjunction with the higher hydrogen-bond interaction of IHL and OHL water molecules promotes greater mobility and self-diffusivity in the monolayer for anatase (101) [39].

When it comes to inter-layer mobility, focusing especially on exchange events between the IHL and OHL density layers, this higher hydrogen bond interaction at anatase (101) is only maximized when joined by a considerably more mobile IHL or OHL layer for longer sub-intervals (cf. Table 2), affording a greater probability of such exchanges to take place [41] (cf. Figure 4b). The dissociative adsorption of individual water molecules on anatase (101) and (b) rutile (110) surface at either IHL and OHL is illustrated in Figure S6a in the Supplementary Information. It is seen how hydrogen bonds between both water molecules' hydrogen atoms H_w and the two neighboring Ob surface atoms of anatase (101) are arranged in the surface. This is, perhaps, one of the reasons anatase (101) presents this 'triple-peak' characteristic, moving slowly in the IHL, but quickly in the OHL at the water- TiO_2 contact.

On a 300 ps time scale, the computed squared displacement of molecules identified in the first adsorbed layers of anatase (101) for longer sub-intervals is showed in Figure 5. Anatase (101) continues to exhibit expected behaviour for IHL and OHL mobility; not differing much of the diffusion seen in shorter 50 ps intervals (cf. Figure S3a in Supplementary information) and moving relatively more in the OHL. Although one can argue some individual molecules identified in the IHL apparently present high diffusivity or are somehow too far from the interface, such as molecule I126,—see snapshots taken at different

times over the trajectory in Figure 6; the authors clarify that molecules may migrate during the overall analysis period and after some period of time might drift relatively far from where they are expected to be. However, the LOP-based layer definition method can assure these are “layer-like” for most of the course of the simulation via significance testing. The authors believe that individual-molecule analysis has been a relatively overlooked field of study in the vast universe of transport properties, as the importance of heterogeneity in molecular characteristics at these layered interfaces has been somehow neglected up to this point. In any event, this study shows the importance of mobility analysis of individual molecules sampled regions, making sure to keep the minimum MSD length for convergence and proper investigation of self-diffusivity.

4. Conclusions

The interfacial structures and mobility of water on the TiO₂ rutile (110) and anatase (101) surfaces have been investigated in this study. The presented results show that this interaction of water with these surfaces has distinct effects at the diverse adsorbed layers of water–TiO₂ interface. As one might expect, anatase (101) exhibited water diffusivity values appreciably greater within the OHL over 300 ps sub-intervals, which could also be noticed in shorter length of MSD for 50 ps intervals. This is believed to be the reason of anatase (101)’s greater photo-activity when compared with rutile (110), since it provides an easier access of water molecules to the anatase (101) surface, and it makes the photo-excited holes at surface interact considerably more, as previously reported in [40]. Interesting high values of individual water molecules self-diffusivities at rutile (110) surface were observed at OHL in specific shorter 50 ps intervals; values even greater than those found for anatase (101) OHL. These findings were somewhat unexpected for this surface structure, as the presence of bridging oxygen in rutile (110) would reduce diffusion motion of this layer along the surface when compared with anatase (101). However, when considering longer 300 ps intervals, rutile (110) OHL presented diffusivities values lower than anatase (101) OHL in all sub-intervals, presumably due to now complete binding or motion that was later negated due to the short 50 ps intervals. These results agree well with literature [41], considering rutile (110) surface plane formed by Ti_{5c} rather than the bridging oxygen atoms Ob.

By way of outlook for future challenges and given the presence of chemically adsorbed water at both interfaces at 298 K as often observed experimentally [2], this shows the importance of understanding both the structural and dynamic behavior of water–TiO₂ interfaces. Indeed, being able to provide further insight into mechanistic coupling of water molecules with metal-oxide surfaces is important, including the overlap of lattice phonon modes with water molecules’ acoustic and optic translational modes; [38–41,58] in this respect, knowing this also enhances the ability for the more accurate modelling of photo- excited-state thermal coupling to optimize photoelectrochemical water-splitting. In this lattice-water thermal the coupling of water molecules’ diffusive motion, including hydrogen-bond rearrangements [41], serves to the boost photocatalytic activity. In this sense, this provides further understanding of the mobility using methods of identification capable to manage physico-chemical abnormality of these surfaces’ topographies more precisely, especially in non-equilibrium layer phases found in the interface region of liquid water [2,30,59], which have extreme importance in energy conversion and in the nanoscale phenomena.

Supplementary Materials: The following supporting information can be downloaded at: <https://www.mdpi.com/article/10.3390/cryst12030398/s1>, Table S1: Self-diffusivities [$\times 10^{-9} \text{ m}^2 \text{ s}^{-1}$] (x,y,z) in adsorbed layer (IHL) and second layer (OHL) from each surface over the first 50 ps of 300 ps sub-intervals. Note that the sum of the different laboratory directions gives the total self-diffusivity. That of bulk water is $\sim 2.23 \times 10^{-9} \text{ m}^2 \text{ s}^{-1}$ whilst the experimental bulk-water value is $2.3 \times 10^{-9} \text{ m}^2 \text{ s}^{-1}$; Table S2: Self-diffusion D (m^2/s) for anatase (101) and rutile (110) at different 50 ps sub-intervals from 100 to 300 ps; Figure S1: Average hydrogen bonds of different adsorbed layers; Figure S2: Probability distribution of self-diffusion coefficients of each individual water molecule in the OHL averaged over a 50 ps sub-interval (450 to 500 ps) for (a) rutile, (b) anatase

diffusivities of the x , y , z directions are shown in blue, red and green dashed lines, respectively. The total diffusivity of individual molecules is represented by the solid black line. Although this sub-interval showed rather unexpected results in the OHL, the other intervals presented distributions similar to those in the 300 ps sub-intervals; Figure S3: Mean square displacement (MSD) of water molecules in different layers at the water-TiO₂ (a) anatase (101) and (b) rutile (110) interface for the interval of 350 and 400 ps. The self-diffusivity experimental bulk-water value of $2.3 \times 10^{-9} \text{ m}^2 \text{ s}^{-1}$ is represented by the grey dotted line for reference; Figure S4: Velocity auto-correlation function of adsorbed layers of rutile (110); Figure S5: Probability distribution of self-diffusion coefficients of each individual water molecule averaged over 50 ps sub-intervals for rutile (110) IHL. Water molecules are considerably sluggish in the IHL for all 50 ps sub-intervals; Figure S6: Dissociative adsorption of water on (a) anatase (101) and (b) rutile (110) surface considering full monolayer coverage. The water molecule on left-side panels consequently split to OH⁻ that adsorbs on Ti_{5c} and H⁺ adsorbing on O_{2c}/O_b (right-side panels). Titanium atoms are shown in light blue, water hydrogen in white, and oxygen atoms from both TiO₂ and water in red. The dashed blue lines represent hydrogen bonds.

Author Contributions: Conceptualization, S.J.B. and N.J.E.; methodology, S.J.B., Y.K. and D.O.; software, D.O., Y.K. and S.J.B.; validation, S.J.B., D.O. and N.J.E.; formal analysis, S.J.B. and D.O.; investigation, S.J.B. and D.O.; resources, R.L.; data curation, S.J.B. and D.O.; writing—original draft preparation, S.J.B.; writing—review and editing, D.O., N.J.E. and R.L.; visualization, S.J.B. and D.O.; supervision, N.J.E.; project administration, N.J.E.; funding acquisition, N.J.E. and R.L. All authors have read and agreed to the published version of the manuscript.

Funding: This research was funded by Science Foundation Ireland grant number SFI-NSFC/17/2259 and NSFC—the bilateral Ireland–China research grant. Run Long acknowledges the National Natural Science Foundation of China (Grant No. 51861135101).

Institutional Review Board Statement: Not applicable.

Informed Consent Statement: Not applicable.

Data Availability Statement: Not applicable.

Acknowledgments: The authors thanks Science Foundation Ireland (SFI-NSFC/17/2259). R. L. acknowledges National Natural Science Foundation of China (grant no. 51861135101).

Conflicts of Interest: The authors declare no conflict of interest.

References

1. Fujishima, A.; Honda, K. Electrochemical Photolysis of Water at a Semiconductor Electrode. *Nature* **1972**, *238*, 37–38. [[CrossRef](#)] [[PubMed](#)]
2. Diebold, U. The surface science of titanium dioxide. *Surf. Sci. Rep.* **2003**, *48*, 53–229. [[CrossRef](#)]
3. Henderson, M.A. A surface science perspective on TiO₂ photocatalysis. *Surf. Sci. Rep.* **2011**, *66*, 185–297. [[CrossRef](#)]
4. Bourikas, K.; Kordulis, C.; Lycourghiotis, A. Titanium Dioxide (Anatase and Rutile): Surface Chemistry, Liquid–Solid Interface Chemistry, and Scientific Synthesis of Supported Catalysts. *Chem. Rev.* **2014**, *114*, 9754–9823. [[CrossRef](#)]
5. Park, N.-G.; van de Lagemaat, J.; Frank, A.J. Comparison of Dye-Sensitized Rutile- and Anatase-Based TiO₂ Solar Cells. *J. Phys. Chem. B* **2000**, *104*, 8989–8994. [[CrossRef](#)]
6. Pang, C.L.; Lindsay, R.; Thornton, G. Structure of Clean and Adsorbate-Covered Single-Crystal Rutile TiO₂ Surfaces. *Chem. Rev.* **2013**, *113*, 3887–3948. [[CrossRef](#)]
7. Kavan, L.; Grätzel, M.; Gilbert, S.E.; Klemen, C.; Scheel, H.J. Electrochemical and Photoelectrochemical Investigation of Single-Crystal Anatase. *J. Am. Chem. Soc.* **1996**, *118*, 6716–6723. [[CrossRef](#)]
8. Zhao, Z.-Y.; Li, Z.; Zou, Z. Surface properties and electronic structure of low-index stoichiometric anatase TiO₂ surfaces. *J. Phys. Condens. Matter* **2010**, *22*, 175008. [[CrossRef](#)]
9. Zhang, H.; Banfield, J.F. Thermodynamic analysis of phase stability of nanocrystalline titania. *J. Mater. Chem.* **1998**, *8*, 2073–2076. [[CrossRef](#)]
10. Ranade, M.R.; Navrotsky, A.; Zhang, H.Z.; Banfield, J.; Elder, S.H.; Zaban, A.; Borse, P.; Kulkarni, S.K.; Doran, G.; Whitfield, H.J. Energetics of nanocrystalline TiO₂. *Proc. Natl. Acad. Sci. USA* **2002**, *99*, 6476–6481. [[CrossRef](#)]
11. Pang, C.L.; Lindsay, R.; Thornton, G. Chemical reactions on rutile TiO₂ (110). *Chem. Soc. Rev.* **2008**, *37*, 2328–2353. [[CrossRef](#)]
12. Mattioli, G.; Filippone, F.; Caminiti, R.; Bonapasta, A.A. Short Hydrogen Bonds at the Water/TiO₂ (Anatase) Interface. *J. Phys. Chem. C* **2008**, *112*, 13579–13586. [[CrossRef](#)]
13. Kumar, N.; Neogi, S.; Kent, P.R.C.; Bandura, A.; Kubicki, J.; Wesolowski, D.J.; Cole, D.; Sofo, J. Hydrogen Bonds and Vibrations of Water on (110) Rutile. *J. Phys. Chem. C* **2009**, *113*, 13732–13740. [[CrossRef](#)]

14. Russo, D.; Teixeira, J.; Kneller, L.; Copley, J.R.D.; Ollivier, J.; Perticaroli, S.; Pellegrini, E.; Gonzalez, M.A. Vibrational Density of States of Hydration Water at Biomolecular Sites: Hydrophobicity Promotes Low Density Amorphous Ice Behavior. *J. Am. Chem. Soc.* **2011**, *133*, 4882–4888. [[CrossRef](#)] [[PubMed](#)]
15. Zhang, Z.; Fenter, P.; Cheng, L.; Sturchio, N.C.; Bedzyk, M.J.; Předota, M.; Bandura, A.; Kubicki, J.D.; Lvov, S.N.; Cummings, P.T.; et al. Ion Adsorption at the Rutile–Water Interface: Linking Molecular and Macroscopic Properties. *Langmuir* **2004**, *20*, 4954–4969. [[CrossRef](#)] [[PubMed](#)]
16. Parez, S.; Předota, M.; Machesky, M. Dielectric Properties of Water at Rutile and Graphite Surfaces: Effect of Molecular Structure. *J. Phys. Chem. C* **2014**, *118*, 4818–4834. [[CrossRef](#)]
17. Předota, M.; Bandura, A.; Cummings, P.; Kubicki, J.; Wesolowski, D.J.; Chialvo, A.; Machesky, M.L. Electric Double Layer at the Rutile (110) Surface. 1. Structure of Surfaces and Interfacial Water from Molecular Dynamics by Use of ab Initio Potentials. *J. Phys. Chem. B* **2004**, *108*, 12049–12060. [[CrossRef](#)]
18. Předota, M.; Zhang, Z.; Fenter, P.; Wesolowski, D.J.; Cummings, P. Electric Double Layer at the Rutile (110) Surface. 2. Adsorption of Ions from Molecular Dynamics and X-ray Experiments. *J. Phys. Chem. B* **2004**, *108*, 12061–12072. [[CrossRef](#)]
19. Předota, M.; Cummings, P.; Wesolowski, D.J. Electric Double Layer at the Rutile (110) Surface. 3. Inhomogeneous Viscosity and Diffusivity Measurement by Computer Simulations. *J. Phys. Chem. C* **2007**, *111*, 3071–3079. [[CrossRef](#)]
20. Mamontov, E.; Wesolowski, D.J.; Vlcek, L.; Cummings, P.T.; Rosenqvist, J.; Wang, W.; Cole, D.R. Dynamics of Hydration Water on Rutile Studied by Backscattering Neutron Spectroscopy and Molecular Dynamics Simulation. *J. Phys. Chem. C* **2008**, *112*, 12334–12341. [[CrossRef](#)]
21. Mamontov, E.; Vlcek, L.; Wesolowski, D.J.; Cummings, P.T.; Rosenqvist, J.; Wang, W.; Cole, D.R.; Anovitz, L.M.; Gasparovic, G. Suppression of the dynamic transition in surface water at low hydration levels: A study of water on rutile. *Phys. Rev. E* **2009**, *79*, 051504. [[CrossRef](#)] [[PubMed](#)]
22. English, N.J.; Waldron, C.J. Perspectives on external electric fields in molecular simulation: Progress, prospects and challenges. *Phys. Chem. Chem. Phys.* **2015**, *17*, 12407–12440. [[CrossRef](#)] [[PubMed](#)]
23. Boyd, S.J.; English, N.J. Influence of external static and oscillating electric fields on self-diffusion of water from molecular dynamics. *J. Mol. Liq.* **2020**, *327*, 114788. [[CrossRef](#)]
24. Nandi, P.K.; English, N.J. Role of hydration layer in dynamical crossover in proteins: Insights from translational self-diffusivity. *J. Phys. Chem. B* **2016**, *120*, 12031. [[CrossRef](#)]
25. Agosta, L.; Brandt, E.G.; Lyubartsev, A.P. Diffusion and reaction pathways of water near fully hydrated TiO₂ surfaces from ab initio molecular dynamics. *J. Chem. Phys.* **2017**, *147*, 024704. [[CrossRef](#)] [[PubMed](#)]
26. Swope, W.C.; Andersen, C.; Berens, P.H.; Wilson, K.R. A computer simulation method for the calculation of equilibrium con-constants for the formation of physical clusters of molecules: Application to small water clusters. *J. Chem. Phys.* **1982**, *76*, 637–649. [[CrossRef](#)]
27. Essmann, U.; Perera, L.; Berkowitz, M.L.; Darden, T.; Lee, H.; Pedersen, L.G. A smooth particle mesh Ewald method. *J. Chem. Phys.* **1995**, *103*, 8577–8593. [[CrossRef](#)]
28. O’carroll, D.; Martinez-Gonzalez, J.A.; English, N.J. Coherency spectral analysis of interfacial water at TiO₂ surfaces. *Mol. Simul.* **2020**, *48*, 1–10. [[CrossRef](#)]
29. Allen, M.P.; Tildesley, D.J. *Computer Simulation of Liquids*; Oxford University Press: Oxford, UK, 2017.
30. Wu, Y.; Tepper, H.; Voth, G.A. Flexible simple point-charge water model with improved liquid-state properties. *J. Chem. Phys.* **2006**, *124*, 024503. [[CrossRef](#)] [[PubMed](#)]
31. Mahoney, M.W.; Jorgensen, W.L. Diffusion constant of the TIP5P model of liquid water. *J. Chem. Phys.* **2001**, *114*, 363. [[CrossRef](#)]
32. Fernández, R.G.; Abascal, J.; Vega, C. The melting point of ice Ih for common water models calculated from direct coexistence of the solid-liquid interface. *J. Chem. Phys.* **2006**, *124*, 144506. [[CrossRef](#)] [[PubMed](#)]
33. Kavathekar, R.S.; Dev, P.; English, N.J.; MacElroy, J. Molecular dynamics study of water in contact with the TiO₂ rutile-110, 100, 101, 001 and anatase-101, 001 surface. *Mol. Phys.* **2011**, *109*, 1649–1656. [[CrossRef](#)]
34. Kavathekar, R.S.; English, N.J.; MacElroy, J.M.D. Study of Translational, Librational and Intra-molecular Motion of Adsorbed Liquid Monolayers at Various TiO₂ Interfaces. *Mol. Phys.* **2011**, *109*, 2645–2654. [[CrossRef](#)]
35. Kavathekar, R.S.; English, N.J.; MacElroy, J. Spatial distribution of adsorbed water layers at the TiO₂ rutile and anatase interfaces. *Chem. Phys. Lett.* **2012**, *554*, 102–106. [[CrossRef](#)]
36. English, N.J.; Kavathekar, R.S.; MacElroy, J.M.D. Hydrogen Bond Dynamical Properties of Adsorbed Liquid Water Monolayers with Various TiO₂ Interfaces. *Mol. Phys.* **2012**, *110*, 2919–2925. [[CrossRef](#)]
37. English, N.J. Diffusivity and Mobility of Adsorbed Water Layers at TiO₂ Rutile and Anatase Interfaces. *Crystals* **2015**, *6*, 1. [[CrossRef](#)]
38. Matsui, M.; Akaogi, M. Molecular Dynamics Simulation of the Structural and Physical Properties of the Four Polymorphs of TiO₂. *Mol. Simul.* **1991**, *6*, 239–244. [[CrossRef](#)]
39. Bandura, A.V.; Kubicki, J.D. Derivation of Force Field Parameters for TiO₂–H₂O Systems from ab Initio Calculations. *J. Phys. Chem. B* **2003**, *107*, 11072–11081. [[CrossRef](#)]
40. Futera, Z.; English, N.J. Exploring Rutile (110) and Anatase (101) TiO₂ Water Interfaces by Reactive Force-Field Simulations. *J. Phys. Chem. C* **2017**, *121*, 6701–6711. [[CrossRef](#)]
41. Reinhardt, A.; Doye, J.P.K.; Noya, E.G.; Vega, C. Local order parameters for use in driving homogeneous ice nucleation with all-atom models of water. *J. Chem. Phys.* **2012**, *137*, 194504. [[CrossRef](#)] [[PubMed](#)]

42. Steinhardt, P.J.; Nelson, D.R.; Ronchetti, M. Bond-Orientational Order in Liquids and Glasses. *Phys. Rev. B* **1983**, *28*, 784. [[CrossRef](#)]
43. O'Carroll, D.; English, N.J. Self-ordering water molecules at TiO₂ interfaces: Advances in structural classification. *J. Chem. Phys.* **2020**, *153*, 064502. [[CrossRef](#)]
44. Luzar, A.; Chandler, D. Structure and Hydrogen Bond Dynamics of Water-Dimethyl Sulfoxide Mixtures by Computer Simulations. *J. Chem. Phys.* **1993**, *98*, 8160. [[CrossRef](#)]
45. Lechner, W.; Dellago, C. Accurate determination of crystal structures based on averaged local bond order parameters. *J. Chem. Phys.* **2008**, *129*, 114707. [[CrossRef](#)]
46. Onda, K.; Li, B.; Zhao, J.; Jordan, K.D.; Yang, J.; Petek, H. Wet electrons at the H₂O/TiO₂ (110) surface. *Science* **2005**, *308*, 1154–1158. [[CrossRef](#)] [[PubMed](#)]
47. Zhao, Z.; Li, Z.; Zou, Z. Structure and properties of water on the anatase TiO₂ 101 surface: From single-molecule adsorption to interface formation. *J. Phys. Chem. C* **2012**, *116*, 11054–11061. [[CrossRef](#)]
48. Zhou, G.; Liu, C.; Huang, L. Molecular Dynamics Simulation of First-Adsorbed Water Layer at Titanium Dioxide Surfaces. *J. Chem. Eng. Data* **2018**, *63*, 2420–2429. [[CrossRef](#)]
49. Lamanna, R.; Delmelle, M.; Cannistraro, S. Role of hydrogen-bond cooperativity and free-volume fluctuations in the non-Arrhenius behavior of water self-diffusion: A continuity-of-states model. *Phys. Rev. E* **1994**, *49*, 2841–2850. [[CrossRef](#)] [[PubMed](#)]
50. Levchenko, A.A.; Kolesnikov, A.I.; Ross, N.L.; Boerio-Goates, J.; Woodfield, B.F.; Li, G.; Navrotsky, A. Dynamics of Water Confined on a TiO₂ (Anatase) Surface. *J. Phys. Chem. A* **2007**, *111*, 12584–12588. [[CrossRef](#)]
51. Spencer, E.C.; Levchenko, A.A.; Ross, N.; Kolesnikov, A.; Boerio-Goates, J.; Woodfield, B.F.; Navrotsky, A.; Li, G. Inelastic Neutron Scattering Study of Confined Surface Water on Rutile Nanoparticles. *J. Phys. Chem. A* **2009**, *113*, 2796–2800. [[CrossRef](#)]
52. Nosaka, A.Y.; Fujiwara, T.; Yagi, H.; Akutsu, H.; Nosaka, Y. Characteristics of Water Adsorbed on TiO₂ Photocatalytic Systems with Increasing Temperature as Studied by Solid-State ¹H NMR Spectroscopy. *J. Phys. Chem. B* **2004**, *108*, 9121–9125. [[CrossRef](#)]
53. Rastogi, A.; Suresh, A.K.; Ghosh, S.J. *Thermodynamics: Physical Chemistry of Aqueous Systems*; InTech: London, UK, 2011; pp. 351–364.
54. McDonnell, K.A.; Wadnerkar, N.; English, N.J.; Rahman, M.; Dowling, D. Photo-active and optical properties of bismuth ferrite (BiFeO₃): An experimental and theoretical study. *Chem. Phys. Lett.* **2013**, *572*, 78–84. [[CrossRef](#)]
55. Ghaani, M.R.; Kusalik, P.G.; English, N.J. Massive generation of metastable bulk nanobubbles in water by external electric fields. *Sci. Adv.* **2020**, *6*, eaaz0094. [[CrossRef](#)]
56. Smith, W.; Forester, T.R. DL-POLY-2.0: A general-purpose parallel molecular dynamics simulation package. *J. Mol. Graph.* **1996**, *14*, 136–141. [[CrossRef](#)]
57. Sang, L.; Zhang, Y.; Wang, J.; Zhao, Y.; Chen, Y. Correlation of the depletion layer with the Helmholtz layer in the anatase TiO₂-H₂O interface via molecular dynamics simulations. *Phys. Chem. Chem. Phys.* **2016**, *18*, 15427–15435. [[CrossRef](#)] [[PubMed](#)]
58. Andrade, M.F.C.; KoHsin, Y.; Zhang, L.; Car, R.; Selloni, A. Free energy of proton transfer at the water-TiO₂ interface from: Ab initio deep potential molecular dynamics. *Chem. Sci.* **2020**, *11*, 2335. [[CrossRef](#)] [[PubMed](#)]
59. Gala, F.; Agosta, L.; Zollo, G. Water Kinetics and Clustering on the (101) TiO₂ Anatase Surface. *J. Phys. Chem. C* **2016**, *120*, 450–456. [[CrossRef](#)]